Non-Reciprocal Lithium Niobate-on-Silicon Acoustoelectric Delay Lines

Hakhamanesh Mansoorzare[1] and Reza Abdolvand
Department of Electrical and Computer Engineering, University of Central Florida, USA
[1]hakha@knights.ucf.edu

***Abstract*—This work demonstrates the first implementation of lithium niobate-on-silicon (LNoSi) non-reciprocal acoustic delay lines (ADL) with tunable insertion loss (IL) utilizing the acoustoelectric (AE) effect. Due to the AE effect, the direction- and the intensity-dependent momentum exchange between the drifting electrons in the Si layer and the acoustic phonons can be utilized to break the intrinsic reciprocity of the ADLs in order to control their frequency response. A 5.2 dB improvement in the IL and a 14.2 dB increase in the reverse isolation (i.e. a 19.4 dB non-reciprocal transmission ratio) is achieved through injecting a 400 µA current in one of the ADLs presented here. This opens up possibilities of merging long delays, tunable attenuators, and switches in a single miniaturized device which is a critical stepping stone in fulfillment of full-duplexed microwave systems.**

***Keywords*—acoustic delay line, acoustoelectric effect, Lamb wave, lithium niobate, non-reciprocal.**

I. Introduction

While the revolution in electronics mainly relied on silicon (Si) and it continues to be driven by it, lithium niobate (LN) is playing the same role in the integrated photonics field. As a result, hybrid electro-optic devices will likely be realized on LN on Si (LNoSi) heterogeneous platforms [1]. Furthermore, due to its outstanding piezoelectric properties, LN has been long studied and employed in radio frequency (RF) acoustics for signal processing applications. More specifically, a great deal of research on the acoustoelectric (AE) phenomenon was fuelled once LN-semiconductor heterostructures were preceded by piezoelectric semiconductor materials as the testbed for studying such phenomenon in the 1960s [2], [3]. AE effect was initially observed in the form of the attenuation of acoustic phonons in an electron plasma as a result of the momentum transfer from former to latter; eventually, it was employed in surface acoustic wave (SAW) AE amplifiers by drifting electrons faster than the phase velocity of the acoustic waves (AW) in a manner similar to a travelling-wave-tube amplifier [4]. However, limited fabrication capabilities at the time and subsequently devices with low efficiency discouraged many researchers from further investigations. It was until recently that advances in wafer-level bonding enabled new demonstrations of the AE effect in heterogeneous SAW structures based on LN [5], [6], [7] while our group demonstrated such effect in thin-film piezoelectric-on-Si (TPoS) Lamb wave resonators [8], [9]. The AE interactions in the latter comprises the piezoelectric coupling as well as the deformation potential, both of which contribute to the anharmonic electron bunching due to the stress in the piezoelectric film and Si layer, respectively [10]. Here, we report on utilizing such interactions in LNoSi platform to realize non-reciprocal Lamb wave acoustic delay lines (ADL) that concurrently allow for tunning the insertion loss (IL) and switching. In this scheme, the inherent reciprocity of such components is broken by the drifting electrons in the underlying Si layer; as it amplifies the signals (i.e. AW) propagating in its direction while attenuating those that propagate in the opposite direction. Such capabilities in a single miniaturized component facilitate the implementation of full-duplexed communications and mitigation of interference in the congested RF spectrum, both of which are essential to the 5G and beyond networks.

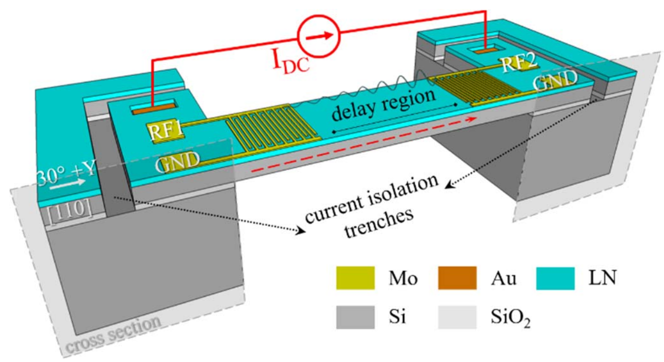

Fig. 1. The conceptual schematic of the proposed device; upon injecting current in the Si layer, AE interactions result in non-reciprocity with respect to the direction of electron flow (dashed red arrow).

II. Design and Implementation of the Device

In order to maximize the AE interactions, a high electromechanical coupling in conjunction with a low concentration of high mobility electrons is desired. To satisfy such conditions, an X-cut LN wafer is directly bonded to a lightly n-type doped 4-inch (100) SOI wafer. The wafers are oriented so that the 30° off +y-axis plane of LN that is commonly known to offer the highest coupling for the symmetric Lamb waves [11] is aligned to the [110] plane of the Si which allows for the highest electron mobility [12]. The device structure is schematically displayed in Fig. 1. The device stack consists of 1 µm LN and 3 µm Si at a doping level of ~7E14 cm^{-3}. Lamb waves are launched by means of 20 pairs of interdigital transducers (IDT) made of a 100 nm-thick molybdenum (Mo) layer from one port and detected at the second port after propagating through the delay region. By utilizing the lateral field excitation, no bottom electrode is incorporated in the device structure. This allows for the strong penetration of the piezoelectrically coupled electric fields into the Si layer and guarantees stronger AE interactions. The IDT finger pitch, defined as the center to center distance between two consecutive electrodes, determines the center of the ADL pass-band and is chosen to be 5 µm herein. The length of the delay region determines the insertion delay (ID) as well as the amount of AE gain and non-reciprocity. In this study, delay lengths of 200 µm (ADL200) and 400 µm (ADL400) are investigated which respectively correspond to 30 ns and 60 ns real-time ID. The lateral boundary of the device is defined by etching the device stack which also restricts the current to pass only through the ADL. In-plane acoustic reflectors [13], [14] are incorporated in one of the configurations (ADL200R) to investigate its effect. In order to pass current through the underlying Si, contacts are formed by etching the LN film and depositing gold (Au) and the ADL is suspended by etching the backside handle layer. The scanning electron micrograph (SEM) of a fabricated device and its IDT is shown in Fig. 2.

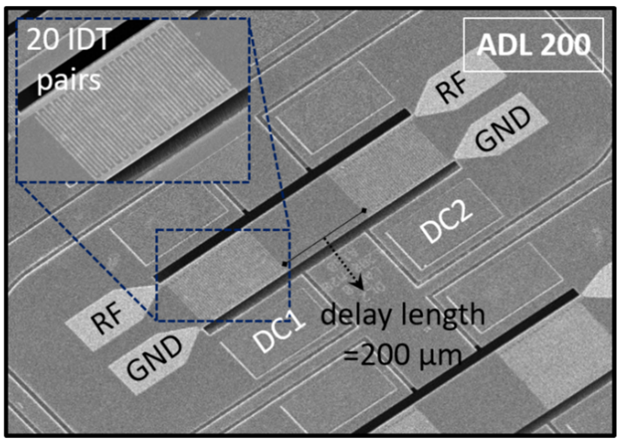

Fig. 2. SEM of ADL200 with its corresponding electrical connections labeled; the inset shows the close up view of the IDTs having 5 µm finger pitch.

In this work, the current values passing through the device are mainly evaluated since they directly impact the AE interactions. By doing so, the parasitic effects of non-Ohmic junctions between Au and lightly n-Si is mostly avoided. Depending on the current intensity and direction, the propagating AWs can be attenuated or amplified along the ADL from one port to another with the AE gain expression being

$$G_{AE} = \mathrm{e}^{\alpha L} \quad (1)$$

where α is the incremental gain coefficient, and L is the device length. The incremental gain is generally expressed [15] in the form of

$$\alpha / k_0 = \frac{K^2}{2} \frac{\gamma \omega \tau}{1+(\gamma \omega \tau)^2}. \quad (2)$$

where k_0 and ω are the wavenumber and angular frequency, K^2 is the electromechanical coupling, γ is the relative difference between the electron drift velocity and AW phase velocity, and τ is a time constant that is determined by the conductivity and permittivity of the structure. It can be inferred from (1) that ideally the longer the ADL, the more AE gain and subsequently loss compensation is achievable. This directly translates to longer ID with lower IL; assuming that the AE gain overcompensates for the propagation loss which has been reported to be ~1 dB.mm^{-1} in such class of LN ADLs [16] while Si is a very low acoustic loss material, as well.

III. Experimental Results

The devices are characterized at normal temperature and pressure by a vector network analyzer (Rhode & Schwarz ZNB 8 VNA) using ground signal ground (GSG) microprobes (Cascade Microtech Inc.) after performing on chip short-open-load-thru calibration to move the reference plane to the microprobe tips. Meanwhile, a pair of DC probes are used to feed the ADL with a voltage source with a controlled current (I_{DC}). Fig. 3 shows the measured frequency response (magnitude of the S-parameters) of ADL200 terminated to 50 Ω (Fig. 3a) and a conjugately matched load (Fig. 3b) prior to passing I_{DC}. It is clear that the ADL shows reciprocity and the fractional bandwidth (FBW) is measured to be 2.1% while the IL is 19.2 dB and 16.5 dB before and after performing the single stage low pass LC matching using the Keysight ADS software, respectively.

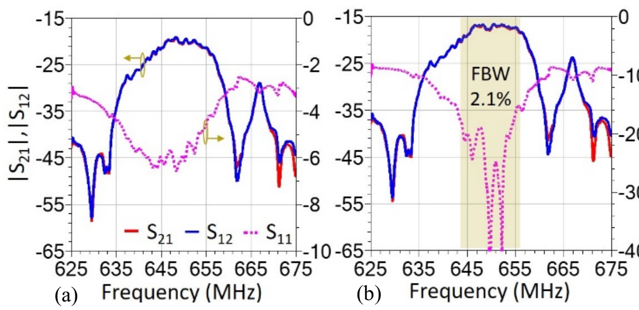

Fig. 3. Frequency response of ADL200 measured prior to current injection (a) while the ports are terminated to 50 Ω and (b) the terminations are conjugate match of the ports of the device.

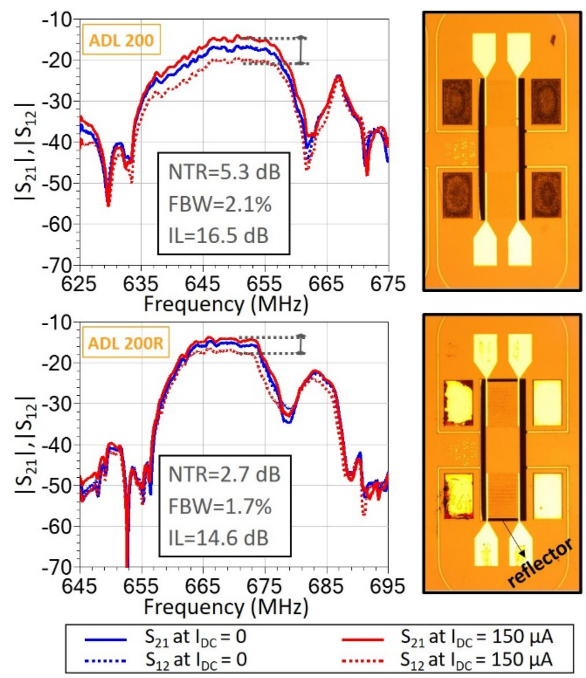

Fig. 4. Frequency response of ADL200 and ADL200R where the blue curves correspond to I_{DC} = 0 µA and the red ones to I_{DC} = 150 µA; solid and dashed lines are respectively S_{21} and S_{12}.

Next, I_{DC} is passed through the ADLs while their RF characteristics is measured. The IL is improved once the electron drift is in the same direction as the propagating RF signal while the reverse isolation is also enhanced due to the AE attenuation of backscattering waves. Fig. 4 compares the magnitude of S_{21} and S_{12} of the ADL200 and ADL200R before and after passing $I_{DC} = 150$ µA through them. While the S_{21} and S_{12} overlap without passing the current, such amount of current results in a non-reciprocal transmission ratio (NTR = $|S_{21}|/|S_{12}|$) of 5.3 dB and 2.7 dB, respectively. Terminating the ADL with the acoustic reflector improves the IL at the expense of reducing the attainable NTR. Fig. 5. displays the transmission and reverse isolation of ADL400 as the injected current it increased from 0 to 400 µA. The IL and NTR of the ADL is tunable by changing the I_{DC}, yielding a 5.2 dB enhancement in the IL with a 19.4 dB of NTR at $I_{DC} = 400$ µA. Additionally, with reversing the current flow, the direction of the changes in the S_{21} and S_{12} is reversed and the ADL is virtually switched off at such current. The measured peak S_{21} and S_{12} of the devices studied herein for a current sweep from 0 to 250 µA is plotted in Fig. 6, confirming that a larger AE gain and NTR is achievable in the longer ADL.

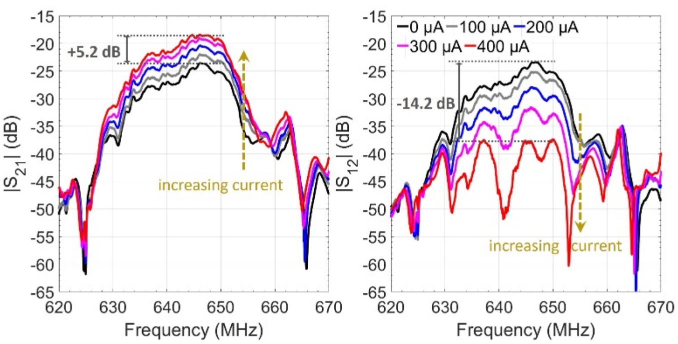

Fig. 5. Frequency response ($|S_{21}|$ on the left and $|S_{12}|$ on the right) of ADL400 terminated to 50 Ω for increasing the I_{DC} from 0 to 400 µA.

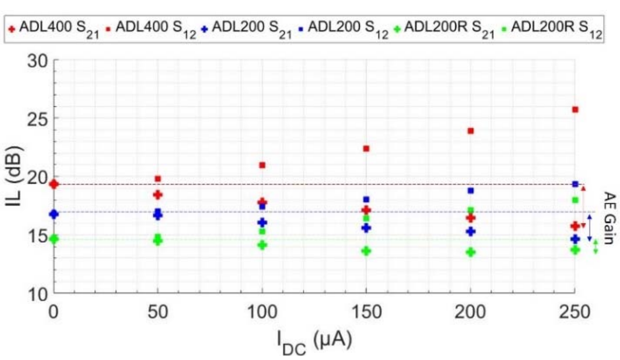

Fig. 6. The IL measured from the peak S_{21} and S_{12} of different ADL types measured for different values of I_{DC} showing a larger AE gain in ADL400.

IV. Conclusion

In this work we demonstrated that by using the momentum exchange between the acoustic phonons and electrons, i.e. acoustoelectric effect (AE), in lithium niobate on silicon heterostructures, non-reciprocal Lamb wave acoustic delay lines (ADL) are realizable that can provide long delays with switching capabilities in a single miniaturized device. By passing a direct current through the lightly doped Si layer, the insertion loss (IL), reverse isolation, and non-reciprocal transmission ratio (NTR) of the ADLs can be manipulated and at a constant current, a higher tuning range for the IL and NTR is achievable for longer devices.

Acknowledgment

This work was supported by the National Science Foundation (NSF) under award 1810143. The authors wish to thank NGK Insulators for providing the bonded wafer.

References

[1] P. O. Weigel et al. "Bonded thin film lithium niobate modulator on a silicon photonics platform exceeding 100 GHz 3-dB electrical modulation bandwidth." Optics express 26, no. 18 (2018): 23728-23739.

[2] A. R. Hutson, J. H. McFee, and D. L. White. "Ultrasonic amplification in CdS." Physical Review Letters 7, no. 6 (1961): 237.

[3] Y. V. Gulyaev, and V. I. Pustovoit. "Amplification of surface waves in semiconductors." Soviet Phys.—JETP 20 (1965): 1508-1509.

[4] J. H. Collins, K. M. Lakin, C. F. Quate, and H. J. Shaw. "Amplification of acoustic surface waves with adjacent semiconductor and piezoelectric crystals." Applied Physics Letters 13, no. 9 (1968): 314-316.

[5] U. K. Bhaskar, S. A. Bhave, and D. Weinstein. "Silicon acoustoelectronics with thin film lithium niobate." Journal of Physics D: Applied Physics 52, no. 5 (2018): 05LT01.

[6] L. Hackett, A. Siddiqui, D. Dominguez, J. K. Douglas, A. Tauke-Pedretti, T. Friedmann, G. Peake, S. Arterburn, and M. Eichenfield. "High-gain leaky surface acoustic wave amplifier in epitaxial InGaAs on lithium niobate heterostructure." Applied Physics Letters 114, no. 25 (2019): 253503.

[7] S. Ghosh. "FDSOI on Lithium Niobate Using Al_2O_3 Wafer-Bonding for Acoustoelectric RF Microdevices." 2019 20th International Conference on Solid-State Sensors, Actuators and Microsystems & Eurosensors XXXIII (TRANSDUCERS & EUROSENSORS XXXIII). IEEE, 2019.

[8] H. Mansoorzare, R. Abdolvand, and H. Fatemi. "Investigation of Phonon-Carrier Interactions in Silicon-Based MEMS Resonators." 2018 IEEE International Frequency Control Symposium (IFCS). IEEE, 2018.

[9] H. Mansoorzare, and R. Abdolvand. "Acoustoelectric Amplification in Lateral-Extensional Composite Piezo-Silicon Resonant Cavities." 2019 Joint Conference of the IEEE International Frequency Control Symposium and European Frequency and Time Forum (EFTF/IFC). IEEE, 2019.

[10] M. Pomerantz. "Ultrasonic loss and gain mechanisms in semiconductors." Proceedings of the IEEE 53.10 (1965): 1438-1451.

[11] I. E. Kuznetsova, B. D. Zaitsev, S. G. Joshi, and I. A. Borodina. "Investigation of acoustic waves in thin plates of lithium niobate and lithium tantalate." IEEE Transactions on Ultrasonics, Ferroelectrics, and Frequency Control 48, no. 1 (2001): 322-328.

[12] T. Sato, Y. Takeishi, H. Hara, and Y. Okamoto. "Mobility anisotropy of electrons in inversion layers on oxidized silicon surfaces." Physical Review B 4, no. 6 (1971): 1950.

[13] B. P. Harrington, and R. Abdolvand. "In-plane acoustic reflectors for reducing effective anchor loss in lateral–extensional MEMS resonators." Journal of Micromechanics and Microengineering 21, no. 8 (2011): 085021.

[14] H. Mansoorzare, S. Moradian, S. Shahraini, R. Abdolvand, and J. Gonzales. "Achieving the Intrinsic Limit of Quality Factor in VHF Extensional-Mode Block Resonators." In 2018 IEEE International Frequency Control Symposium (IFCS), pp. 1-4. IEEE, 2018.

[15] R. Adler. "Simple theory of acoustic amplification." IEEE Transactions on Sonics and Ultrasonics 18.3 (1971): 115-118.

[16] R. Lu, T. Manzaneque, Y. Yang, M. Li and S. Gong, "Gigahertz Low-Loss and Wideband S0 Mode Lithium Niobate Acoustic Delay Lines," in IEEE Transactions on Ultrasonics, Ferroelectrics, and Frequency Control, vol. 66, no. 8, pp. 1373-1386, Aug. 2019.